

Tropical cyclone activity in nested regional and global grid-refined simulations

Atsushi Hashimoto¹ · James M. Done² · Laura D. Fowler² · Cindy L. Bruyère^{2,3}

Received: 12 February 2015 / Accepted: 24 September 2015 / Published online: 5 October 2015
© The Author(s) 2015. This article is published with open access at Springerlink.com

Abstract The capacity of two different grid refinement methods—two-way limited area nesting and variable-mesh refinement—to capture Northwest Pacific Tropical Cyclone (TC) activity is compared in a suite of single-year continuous simulations. Simulations are conducted with and without regional grid refinement from approximately 100–20 km grid spacing over the Northwest Pacific. The capacity to capture smooth transitions between the two resolutions varies by grid refinement method. Nesting shows adverse influence of the nest boundary, with the boundary evident in seasonal average cloud patterns and precipitation, and contortions of the seasonal mean mid-latitude jet. Variable-mesh, on the other hand, reduces many of these effects and produced smoother cloud patterns and mid-latitude jet structure. Both refinement methods lead to increased TC frequency in the region of refinement compared to simulations without grid refinement, although nesting adversely affects TC tracks through the contorted mid-latitude jet. The variable-mesh approach leads to enhanced TC activity over the Southern Indian and Southwest Pacific basins, compared to a uniform mesh simulation. Nesting, on the other hand, does not appear to influence basins outside the region of grid refinement. This study provides evidence that variable mesh may bring benefits to seasonal TC simulation

over traditional nesting, and demonstrates capacity of variable mesh refinement for regional climate simulation.

Keywords Tropical cyclone · Downscaling · Upscaling · Nesting · Variable mesh

1 Introduction

Capturing the climate of high-impact weather is an important challenge for dynamical models. High-impact phenomena such as Tropical Cyclones (TCs) arise from multi-scale processes that require high-resolution to capture explicitly (Giorgi and Bates 1989; Wang et al. 2004). A few decades ago, Global Climate Models (GCMs) used hundreds-km horizontal grid spacing (e.g., The NCAR Community Climate Model used $4.5^\circ \times 7.5^\circ$, Williamson et al. 1987), and Regional Climate Models (RCMs) used tens-km horizontal grid spacing (e.g., RegCM used 50 km, Hirakuchi and Giorgi 1995). Recently, GCM resolutions have approached that of traditional RCMs. For example, the Meteorological Research Institute Atmospheric General Circulation Model has been run at 20 km grid spacing (Kusunoki et al. 2006), and the NCAR Community Atmosphere Model at 0.25° (Wehner et al. 2014). At these resolutions individual weather systems are well resolved, permitting analysis of global TC activity for example (Wehner et al. 2014). In turn, RCM resolutions increased further (e.g., The Non-Hydrostatic Regional Climate Model with 5 km, Sasaki et al. 2011), permitting simulation of fine-scale dynamical processes at climate timescales (e.g., Kendon et al. 2014).

RCMs have been used extensively to study the influence of climate variability and change on TC activity (e.g., Knutson et al. 2013; Done et al. 2013; Jourdain et al. 2011). High-resolution simulations on global or large limited-area

✉ James M. Done
done@ucar.edu

¹ Central Research Institute of Electric Power Industry, 1646 Abiko, Abiko-shi, Chiba 270-1194, Japan

² National Center for Atmospheric Research, 3090 Center Green Drive, Boulder, CO 80301, USA

³ Environmental Sciences and Management, North-West University, Potchefstroom, South Africa

domains are ultimately limited by computational cost and these costs are particularly severe for long-period climate simulations. Variable resolution global simulations offer a computationally efficient alternative to global high resolution that combines the advantages of global simulation in representing the global circulation with high resolution in regions of interest. Such approaches have shown some success in capturing global and regional climate (Chen et al. 2011; Zarzycki et al. 2015) and also TC statistics (Harris and Lin 2014; Zarzycki and Jablonowski 2014; Fowler et al. 2015), yet the simulation advantages of such an approach over traditional limited area modeling is not well understood.

In this study, the capacity of two different mesh refinement approaches to capture Northwest Pacific TC activity is compared. Specifically, the Advanced Research Weather Research and Forecasting model (WRF-ARW, Skamarock et al. 2008) is used with a tropical channel domain (Done et al. 2013) and compared with the global atmosphere-only Model for Prediction Across Scales (MPAS, Thuburn et al. 2009; Ringler et al. 2010). The impact of horizontal grid refinement over the Northwest Pacific is compared between the models: WRF uses a two-way nesting approach (Michalakes et al. 2004), and MPAS uses a variable resolution mesh (Skamarock et al. 2012). The capacity of each model and refinement method to capture smooth transitions across the grid refined region and the large-scale seasonal climate is demonstrated using large-scale cloud patterns, mid-tropospheric jet structure, and precipitation, and the influence on TC activity is examined. For a case study of the active 2005 North Atlantic TC season, Fowler et al. (2015) demonstrated the capacity of MPAS using mesh refinement over the North Atlantic to capture the frequency and general locations of North Atlantic TCs. This study focuses on TC activity over the Northwest Pacific TC; a region of very different large-scale forcing of TCs and TC formation pathways (McTaggart-Cowan et al. 2013).

The next section describes the methodology, datasets, and an automated TC detection and tracking method. In Sect. 3, sensitivity of the large-scale climate to model and grid refinement method is presented. Section 4 presents differences in TC activity across models and grid refinement methods. Conclusions are drawn in Sect. 5.

2 Methodology

2.1 Model setups

To support this comparison study between two grid refinement approaches, model versions are selected to allow use of the same microphysical parameterizations. MPAS-A version 2.0 and WRF-ARW version 3.5.1 allow for the use

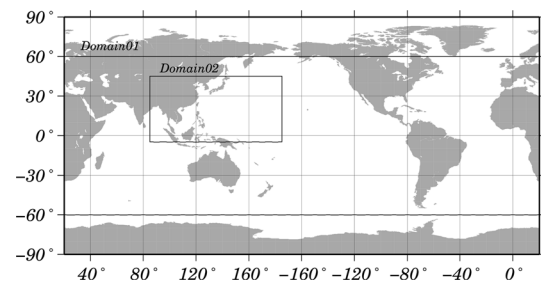


Fig. 1 WRF model computational domains

of common microphysical schemes, though their interaction with grid resolved flow will differ between the models and resolutions. Both models use the Kain-Fritsch cumulus parameterization scheme (Kain 2004), the WSM6 single-moment microphysics scheme (Dudhia et al. 2008), the Yonsei University planetary boundary layer scheme (Hong et al. 2006), the Noah land surface scheme (Chen and Dudhia 2001), and the Community Atmosphere Model (CAM) short and long wave radiation schemes (Collins et al. 2004).

WRF and MPAS are fully compressible non-hydrostatic models. In the horizontal, WRF tropical channel domain is based on latitude-longitude coordinate using Arakawa C-grid, and MPAS is based on unstructured centroidal Voronoi C-grid meshes. In the vertical, WRF tropical channel domain uses a terrain-following hydrostatic-pressure coordinate, and MPAS uses a height-based hybrid smoothed terrain-following coordinate (Klemp et al. 2007). WRF model top is 10 hPa, MPAS model top is 30 km, and both models have 50 vertical levels.

Figure 1 shows the WRF model computational domains that comprise a tropical channel domain (similar to that used by Ray et al. (2011), and referred to hereafter as domain01) and a nested domain (referred to hereafter as domain02) over the Northwest Pacific. Domain01 has dimensions 361×121 grid points and horizontal grid spacing of 1.0° (111 km at the equator). Domain02 has dimensions 501×251 grid points and horizontal grid spacing of 0.2° (22 km at the equator). Domain01 spans 60°S – 60°N with periodic boundary conditions in the east–west direction (Fig. 1), and domain02 covers the main regions of observed TC genesis and TC tracks over the Northwest Pacific basin (85°E – 5°W , 5°S – 45°N). WRF lateral boundary conditions use linear relaxation over five grid points (one specified point and four relaxation points). WRF nesting can operate as both one-way or two-way: two-way allows both downscaling from domain01 to domain02 and upscaling from domain02 to domain01, whereas one-way nesting only permits downscaling. In this study, two-way nesting is used to be consistent with the flow across scales inherent to MPAS.

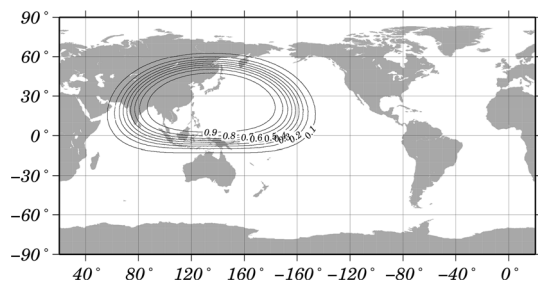


Fig. 2 Mesh density distribution of the global MPAS grid. The high-density region corresponds to high horizontal resolution (mesh density = 1 corresponds to a grid spacing of approximately 23 km), and low-density regions correspond to coarse-resolution (mesh density = 0 corresponds to a grid spacing of approximately 120 km)

This study uses two MPAS grids; a global uniform mesh at 120 km grid spacing (40,962 grid cells), and a global variable resolution mesh (Fig. 2, 153,762 grid cells) with refinement from 120 to 23 km centered over the Northwest Pacific (25°N, 135°E). Model grids are designed such that MPAS and WRF have refinement over a similar region.

A suite of single year simulations are conducted for the period May 1, 2005 to April 30, 2006. Forcing data are derived from NCEP/NCAR Reanalysis project (NNRP, Kalnay et al. 1996) at 2.5° grid spacing for the atmosphere and NOAA Weekly Optimum Interpolation Sea Surface Temperatures (OI-SST, Hurrell et al. 2008) at 1.0° grid spacing. WRF and MPAS use NNRP and OI-SST for initial conditions, and OI-SST for surface boundary conditions. Additionally, WRF domain01 uses NNRP for lateral boundary conditions. All boundary conditions update every 6 h. Qian et al. (2003) showed two timescales of regional climate model spin up; a rapid 1–2 day geostrophic adjustment of the initial mass and wind fields to be in balance with the model dynamics, and a slower 2–3 week adjustment to the state of the model climatology. Although spin up will vary by model and domain size, given that most TC activity takes place after June 1, and our analysis focuses on the period July–August–September, our results should not be significantly impacted by model spin up.

Four simulations are conducted (Table 1) to allow for comparison between models and comparison between uniform resolution and the use of grid refinement. For the WRF model, a simulation using a single tropical channel domain at 1° is referred to hereafter as WRF_D1, and a simulation with an added nest over the Northwest Pacific at 0.2° is referred to as WRF_D2. Hereafter, WRF_D2 is the combination of domain01 and domain02, and treated as one dataset for the analysis. For MPAS, a simulation with a uniform mesh at 120 km is referred to as MPAS_UM and a simulation with mesh refinement over the Northwest Pacific from 120 to 23 km is referred to as MPAS_VM. Multi-year simulations or ensemble simulations of a single

Table 1 Summary of four simulations

Simulation	Domain specifications
WRF_D1	Single tropical channel domain at 1.0°
WRF_D2	Tropical channel domain at 1.0° with Northwest Pacific nest at 0.2°
MPAS_UM	Global uniform mesh at 120 km
MPAS_VM	Global variable mesh with refinement over Northwest Pacific from 120 to 23 km

Refer to Figs. 1 and 2 for WRF and MPAS domain locations. WRF_D2 is the combination of domain01 and domain02, and treated as one dataset for the analysis

year would be necessary to account for internal variability and assess model skill. Rather than assessing the skill of the models, this study focuses on single-year simulations to demonstrate the capacity of a variable resolution mesh for seasonal TC simulation, and identify potential benefits above the nesting approach to mesh refinement.

2.2 Cyclone detection and tracking

TCs are analyzed using an automated TC detection and tracking algorithm based on Suzuki-Parker (2012). This algorithm operates on six hourly model output data from both WRF and MPAS. The detection and tracking of TCs proceeds as follows.

2.2.1 TC detection

The tracker uses the following criteria: (1) Identify a grid point pressure at mean sea level (PMSL) <1020 hPa, PMSL gradient of 2 hPa within 250 km (of the center) and a wind speed >17 ms⁻¹ within 100 km; and (2) if the grid point identified in step (1) is not the minimum PMSL within 500 km, then remove this point and keep the point with the minimum PMSL.

2.2.2 Thermal wind and warm core structure criteria

Thermal wind and warm core structure criteria are applied to the grid points identified above. Step (3) checks that the average magnitude of 850 hPa relative vorticity (within 100 km) is >1.0 × 10⁻⁵s⁻¹ for the northern hemisphere and -1.0 × 10⁻⁵s⁻¹ for the southern hemisphere. Step (4) checks that the sum of horizontal temperature anomalies (defined as average temperature within 100 km minus average temperature within 100–1000 km) at 300, 500, and 700 hPa is >2.0 K. Step (5) checks that the maximum wind speed at 850 hPa is greater than that at 300 hPa within 100 km, and finally, step (6) checks that the horizontal temperature anomaly at 300 hPa is greater than that at 850 hPa (defined as the same as in Step 4)).

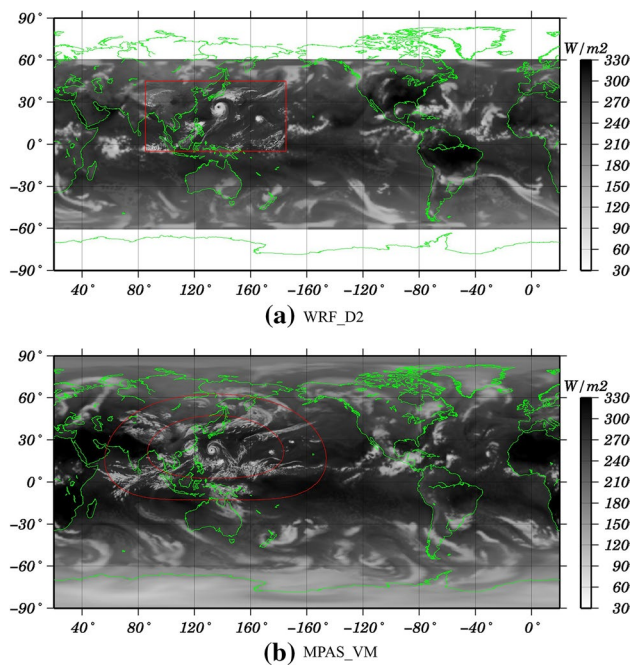


Fig. 3 Outgoing Longwave Radiation (Wm^{-2}) at 1800UTC 15 September 2005 (137 days after initial time), for **a** WRF_D2 (*red solid line* indicates the outer frame of domain02), and **b** MPAS_VM (*red solid lines* indicate inner (mesh density = 0.9) and outer (mesh density = 0.1) regions)

2.2.3 Cyclone thermal symmetry criteria

Using the cyclone phase parameters defined by Hart (2003), the cyclone thermal symmetry is checked to further ensure the detected grid points satisfy the conditions for a warm core and also to provide additional information on the cyclone phase. Step (7) checks that parameters $-|VT_L|$ and $-|VT_U|$ (the cyclone lower and upper tropospheric thermal wind) defined as gradients between 900 and 600 hPa and between 600 and 300 hPa every 50 hPa are greater than zero. Step (8) checks that parameter ‘B’ (a measure of cyclone thermal symmetry defined as the difference of 600–900 hPa thickness to the right and left of track within a 500 km radius) is 10 m or less.

2.2.4 TC tracking

To define a track from sets of cyclone points detected from steps (1) through (8), step (9) uses criteria based on speed and direction defined by Hart (2003) to connect cyclone points into tracks. Step (10) requires all above conditions are met for at least 48 h; step (11) checks for TCs that regenerate, and connects separated tracks using the method in step (10), but includes two direction restrictions. The connection of separated tracks is disallowed when two

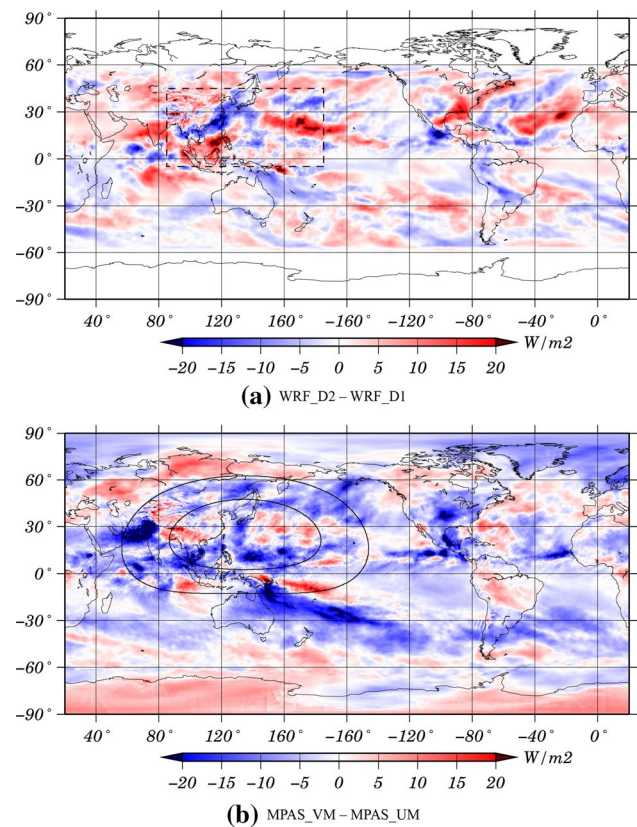


Fig. 4 Mean Outgoing Longwave Radiation (Wm^{-2}) difference between **a** WRF_D2 and WRF_D1, and **b** MPAS_VM and MPAS_UM for July–August–September 2005. The *dashed line* outlines WRF domain02 and the *solid lines* indicate MPAS_VM mesh densities of 0.1 (*outer ellipse*) and 0.9 (*inner ellipse*)

consecutive points are more than 500 km apart with an equatorward change of more than 1.0° and when the SLP of post-connection point is <990 hPa. This restriction prevents connections with newly generated TCs.

3 Sensitivity of seasonal climate to model and grid refinement

WRF uses two-way nesting in which small scales generated on domain02 are temporally and spatially filtered as the domain01 grid points in the region of domain02 are replaced with domain02 information at each domain01 time step. As a result, it is possible that discontinuities at the domain02 boundary could modify weather systems as they transition across the boundary. For MPAS, Skamarock et al. (2012) showed the variable mesh transition zone produced no such problems for the case of 5-day forecasts. Here, the influence of the two grid refinement approaches is explored on seasonal timescales.

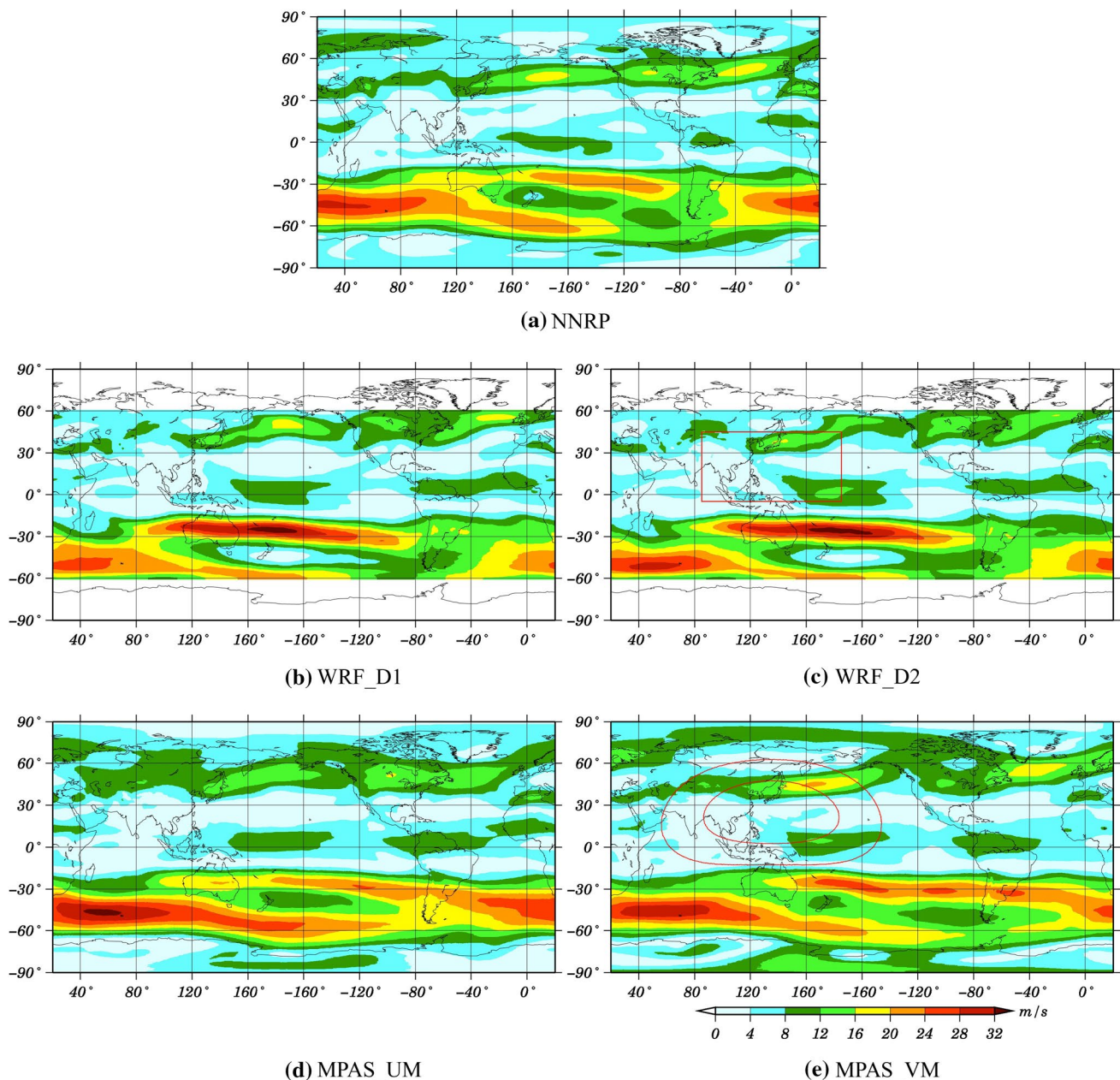


Fig. 5 Seasonal mean wind speed at 500 hPa for July–August–September 2005, for **a** NNRP, **b** WRF_D1, **c** WRF_D2, **d** MPAS_UM, and **e** MPAS_VM

3.1 Cloud patterns

Figure 3 shows OLR for WRF_D2 and MPAS_VM at 18UTC September 15th 2005—a time that had a TC in each simulation. Although there is an abrupt resolution change at the nest boundary, for example over Northeast to Northwest Pacific, Northwest Pacific to Bering Sea, and India Ocean to Southeast Asia, WRF nesting appears to perform reasonably well at capturing smooth transitions in features evident in the cloud patterns at the nest boundary, at least qualitatively. MPAS, that allows gradual change

across scales, also handles well the transition of features within the variable mesh region.

Differences become apparent, however, on longer time-scales. Seasonal mean OLR differences between WRF_D2 and WRF_D1 from July to September (JAS, Fig. 4a) shows abrupt changes along some sections of the nest boundaries, particularly along the southern and eastern boundary. The difference field between MPAS_VM and MPAS_UM (Fig. 4b) on the other hand, does not show any cloud field discontinuities on seasonal timescales across the region of mesh refinement.

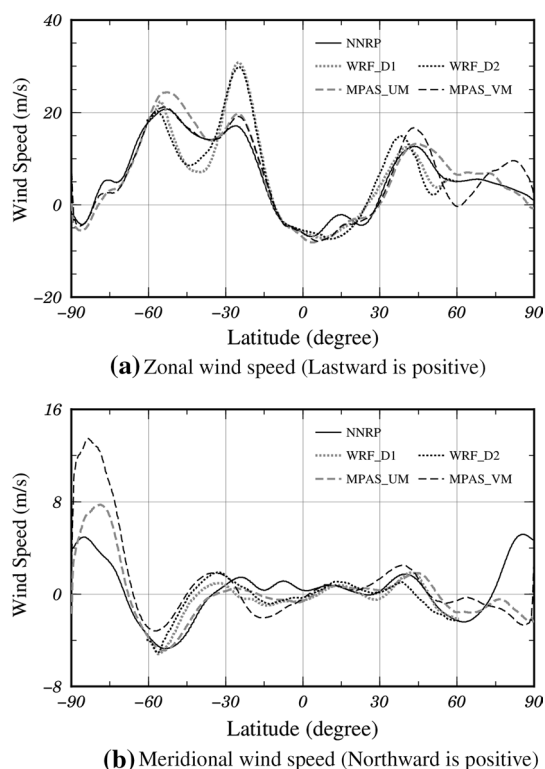


Fig. 6 Seasonal zonal mean wind speed at 500 hPa for July–August–September 2005 between 130°E and 160°E corresponding to the region of grid refinement and the anomalously strong flow over the Southwest Pacific (Fig. 4), for **a** zonal wind speed (Eastward is positive) and **b** meridional wind speed (Northward is positive)

3.2 Mid-latitude jet structure

Figure 5 shows summer (JAS) mean wind speed at 500 hPa for NNRP, WRF_D1, WRF_D2, MPAS_UM, and MPAS_VM. An ensemble or multi-year simulation approach would be needed to make a formal skill assessment, whereas the comparison with NNRP presented here is to demonstrate capacity to capture the major seasonal large-scale flow patterns. The simulated large-scale flows generally compare favorably with NNRP, but with some notable exceptions. At the poles, MPAS simulations deviate substantially from NNRP and among themselves. In WRF_D1 and WRF_D2, anomalously strong large-scale flow is located over the Southwest Pacific Ocean and is likely due to an influence of the fixed southern boundary at 60°S. MPAS, on the other hand, is able to capture a more realistic jet structure over the Southwest Pacific.

Over the Northwest Pacific, the impact of mesh refinement for both WRF and MPAS is an equatorward shift in the westerly jet maxima and an increase in the jet magnitude. For both WRF and MPAS this may be a consequence of the enhanced TC activity in the mesh-refined simulations (shown later in Fig. 9). For WRF_D2, however, the

jet appears to be constrained along the northern boundary of domain02, and then distorts as it exits the region of the nest. MPAS_VM, on the other hand, produces a smooth jet structure with no distortion (Fig. 5).

These flow features can also be seen in the local (between 130°E and 160°E) zonal mean wind speeds at 500 hPa for NNRP and the four simulations (Fig. 6). This longitude band covers the region of grid refinement and the anomalously strong flow over the Southwest Pacific. Again, large-scale variations in the local zonal mean wind speeds compare reasonably well with NNRP, except at the poles. MPAS_UM and MPAS_VM capture the latitudes and approximate magnitudes of the wind speed maxima in the southern mid-latitudes, whereas WRF_D1 and WRF_D2 severely overestimate these peak winds. Again, the jet maxima over northern mid-latitudes is shifted equator-ward and increases in magnitude in the mesh refined simulations compared to uniform mesh simulations for both WRF and MPAS. In addition, the northward flow in WRF_D2 is the weakest among the simulations, suggesting a modification of the jet by the nesting approach.

3.3 Precipitation

Figure 7 shows daily mean (JAS) precipitation for Global Precipitation Climatology Project (GPCP, 1.0° resolution, Adler et al. 2003), Tropical Rainfall Measuring Mission 3B43 (TRMM, 0.25° resolution, Huffman et al. 2007), and the four simulations. Again, comparison with observations is presented here to demonstrate capacity to capture the major seasonal large-scale precipitation patterns rather than to formally assess model skill. To quantify similarity between datasets, the bias and Pearson product-moment correlation coefficients are calculated and presented in Table 2. Although all simulations overestimate precipitation amounts globally by approximately 1.0 mm/day the large-scale spatial precipitation patterns compare favorably with GPCP and TRMM (Table 2).

For the region of the Northwest Pacific, where summer precipitation is dominated by convective systems, the bias of each simulation is slightly higher than the global value and the correlation slightly lower. The effect of grid refinement is to further increase the regional bias for both WRF and MPAS with no substantial change in regional correlation. The high internal variability of TCs (Done et al. 2014) is likely preventing any improvement in regional correlation with mesh refinement.

Figure 8 shows zonal mean daily mean (JAS) precipitation for global and local (between 100°E and 180°E, covering the Northwest Pacific) regions, for GPCP, TRMM, WRF_D2, and MPAS_VM. Although the effects of the relaxation zones at the northern and southern lateral boundaries (60°S, 60°N) and nesting boundary zones (5°S,

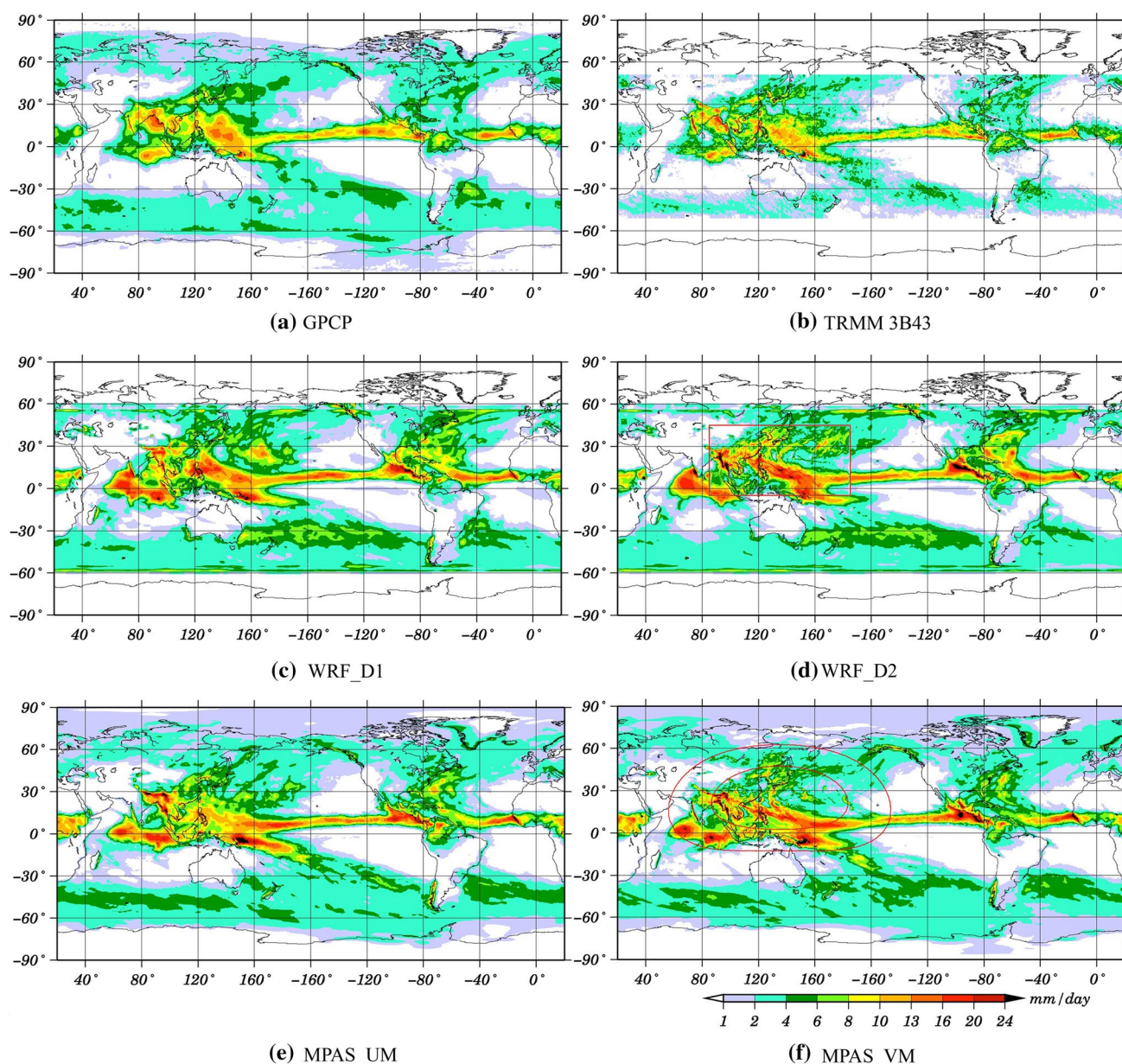


Fig. 7 Mean daily precipitation (mm day^{-1}) for July–August–September 2005, for **a** GPCP, **b** TRMM, **c** WRF_D1, **d** WRF_D2, **e** MPAS_UM, and **f** MPAS_VM

45°N) are evident in WRF_D2, large-scale variations in both the global and local zonal mean total precipitation are generally well captured in WRF_D2 and MPAS_VM compared with GPCP and TRMM. But the amounts are overestimated. From a regional perspective, WRF_D2 overestimates precipitation over the South Pacific around 30°S, corresponding to the southern shear line associated with the anomalously strong large-scale flow at 500 hPa (Fig. 5c). Overestimation is greatest in WRF_D2 and MPAS_VM over tropical regions where convective activity is dominant (Fig. 8c). Figure 7 indicates this overestimation is most pronounced for the coastal areas of continents

and islands, and also in regions of large-scale convergence over the oceans, rather than confined to the region of high resolution.

MPAS_VM is able to produce smooth precipitation features from the East China Sea to Alaska, across the region of refinement (Fig. 7). MPAS_VM captures the jet from East China Sea to Alaska, whereas the jet simulated by WRF_D2 is constrained by lateral and nesting boundaries. It seems likely that both the global domain and smooth transition between fine and coarse resolution for MPAS contribute to the smoother jet structure (shown earlier in Fig. 5) and smoother precipitation features over the

Table 2 Bias and Pearson product-moment correlation coefficient (R) between simulated and TRMM daily average precipitation (mm day⁻¹) over the period July–August–September 2005

	WRF_D1	WRF_D2	MPAS_UM	MPAS_VM
BIAS_45N45S	1.2	1.1	1.0	1.0
BIAS_NWP	1.7	1.9	1.3	1.5
R_45N45S	0.75	0.72	0.77	0.77
R_NWP	0.52	0.53	0.54	0.59

‘_45N45S’ corresponds to the TRMM domain (45°S–45°N, all longitudes), and ‘_NWP’ corresponds to the region of the Northwest Pacific as defined by WRF domain02 (90°E–180°E, 0°N–40°N) that excludes a 5° border region from domain02

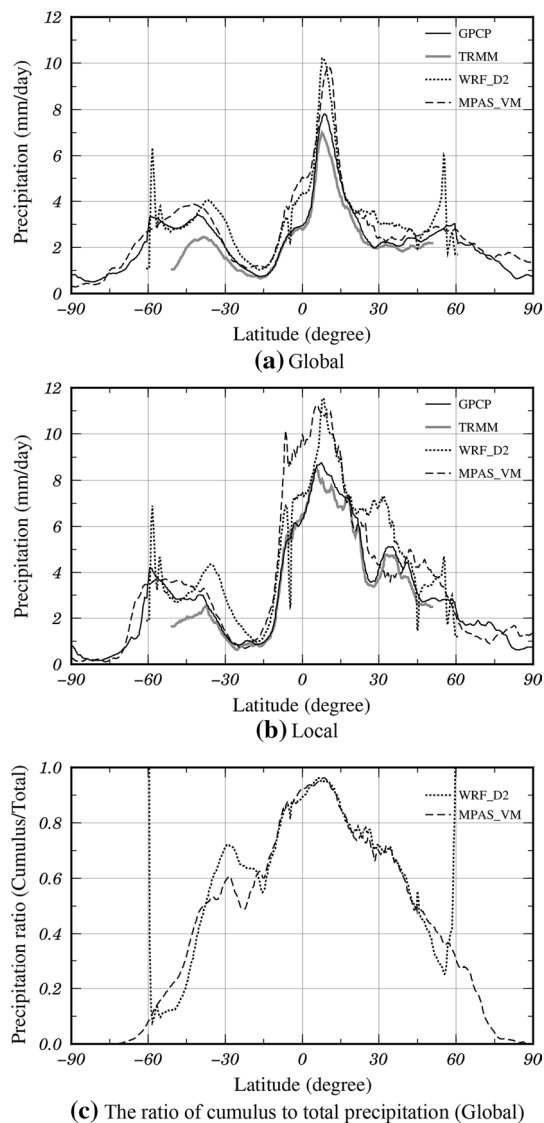


Fig. 8 Seasonal mean daily precipitation for July–August–September 2005, for **a** global zonal average, **b** local zonal average between 100°E and 180°E corresponding to the longitude band of the Northwest Pacific, and **c** the ratio of cumulus to total precipitation

Northwest Pacific compared to WRF (Fig. 7). This smooth transition permits extra-tropical transitioning cyclones to exit the region of refined mesh unimpeded by shocks associated with abrupt resolution of the nesting approach.

4 Sensitivity of tropical cyclone activity to model and grid refinement

The previous section hypothesized that precipitation differences in tropical and subtropical regions may be partly attributed to differences in TC activity. Figure 9 depicts the TC genesis locations and tracks, for observations (International Best Track Archive for Climate Stewardship (IBTrACS) v03r05, Knapp et al. 2010), WRF_D1, WRF_D2, MPAS_UM, and MPAS_VM, from 1 May, 2005 to 30 April, 2006. As expected, regional grid refinement methods (both WRF_D2 and MPAS_VM) increase TC frequency in the region of grid refinement compared to simulations without grid refinement (WRF_D1 and MPAS_UM). Although TC frequencies are generally overestimated in the region of grid refinement (Table 3), the general area of TC genesis points and tracks compares well with IBTrACS. Additionally, MPAS_VM enhances TC activity over the Southern Indian and Southwest Pacific basins, unlike WRF_D2 that does not appear to substantially influence basins outside the region of grid refinement.

Mizuta et al. (2012) showed that modification of cumulus parameterization—specifically, the treatments of entraining and detraining plumes, reducing the conversion rate of cloud water to precipitation, and suppressing the conversion near the cloud bottom—improved simulation of monthly mean precipitation and TC activity over the Northwest Pacific. It is likely that the overestimation of TC frequency and convective rainfall over tropical regions presented here may also be in part attributed to details of the cumulus scheme. Indeed, Bullock et al. (2015) showed a reduced wet bias in TC simulations using WRF by tuning the convective adjustment timescale in the Kain-Fritsch scheme.

To examine the simulation of re-curving TC tracks over the Northwest Pacific (Archambault et al. 2013), Fig. 10 depicts the zonal averaged TC tracks for IBTrACS, WRF_D2, and MPAS_VM. Zonal averaging only uses TCs generated within the region (125°E–160°E, 5°S–25°N, indicated in Fig. 10). The trajectory of the zonal average MPAS_VM track closely follows that of IBTrACS but is shifted to the West by approximately 400 km. The zonal average WRF_D2 track however follows a different trajectory and recurves too early (at lower latitude) compared to IBTrACS and MPAS_VM. As noted in the previous section the westerly jet of WRF_D2 appears to be constrained along the northern domain02 boundary (Fig. 5c), with the jet

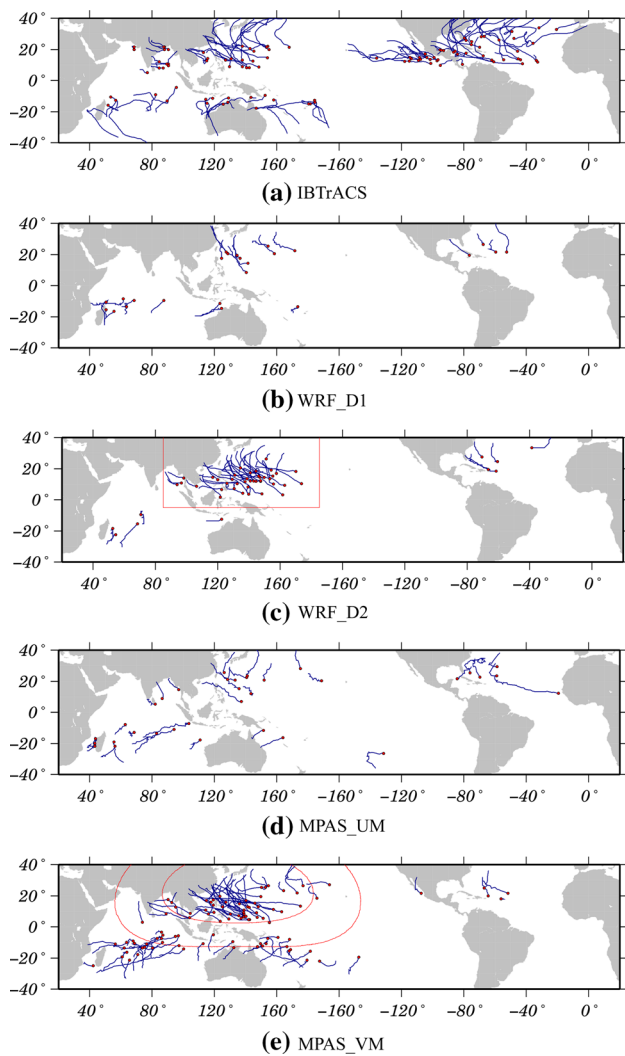


Fig. 9 TC genesis locations (red dots) and TC tracks (blue lines) from May 2005 to April 2006 for **a** IBTrACS, **b** WRF_D1, **c** WRF_D2, **d** MPAS_UM, and **e** MPAS_VM

maximum located further south than in NNRP or MPAS_VM; and, the southerly flow component flow is the weakest of each case (Fig. 6b). This analysis suggests that the deviation of the large-scale flow due to the nesting and lateral boundary conditions adversely affects the mean TC track.

Table 3 TC frequency over each basin for observations and the four simulations from May 2005 to April 2006

	NEP	SEP	NA	SA	NI	SI	NWP	SWP
IBTrACS	15	4	29	0	4	12	20	4
WRF_D1	0	0	4	0	0	9	10	1
WRF_D2	0	0	5	0	3	5	37	0
MPAS_UM	1	1	6	0	3	11	10	2
MPAS_VM	3	3	4	0	5	24	44	14

Northeast Pacific is NEP, Southeast Pacific is SEP, North Atlantic is NA, South Atlantic is SA, North Indian is NI, South Indian is SI, Northwest Pacific is NWP, and Southwest Pacific is SWP

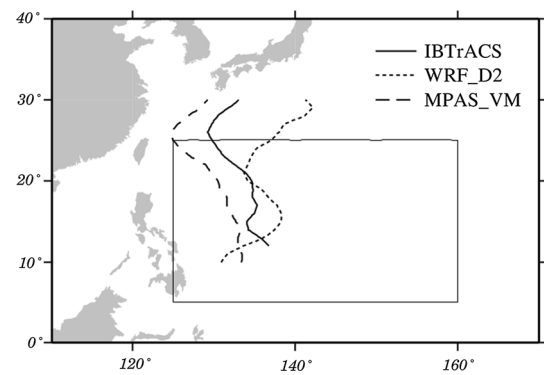


Fig. 10 Zonal mean TC track from 10°N–30°N for IBTrACS, WRF_D2 and MPAS_VM. Only TCs generated within the region (125°E–160°E, 5°S–25°N, indicated by the box outlined with a thin black line) are used for the zonal averaging. Zonal averages are calculated every 1° latitude and smoothed using a five-point moving average

To explore the influence of grid refinement on TC structure, Fig. 11 depicts the relationships between TC minimum pressure at mean sea level (PMSL) and TC maximum 10 m-height TC wind speed over the Northwest Pacific, for all 6-hourly track data points for IBTrACS, WRF_D1, WRF_D2, MPAS_UM, and MPAS_VM. As expected, both grid refinement methods result in stronger wind speeds compared to the simulations without grid refinement, leading to improved wind-pressure relationships compared with IBTrACS. But the grid refinement simulations still miss the most intense observed winds, despite capturing the lowest observed PMSL. MPAS produces lower PMSLs and higher wind speeds than WRF, at both coarse and high resolution. Furthermore, MPAS_VM produced PMSLs lower than observed.

To explore TC intensification rates, Fig. 12 shows time-series of mean TC minimum PMSL after mean genesis time for TCs over the Northwest Pacific, for IBTrACS, WRF_D2, and MPAS_VM. Data are plotted when the averaging sample size is ≥ 10 TCs and for IBTrACS, when wind speed is ≥ 17 m/s for consistency with the definition of simulated TCs. The mean intensification rates and overall intensity evolution in terms of PMSL are reproduced reasonably well for both WRF_D2 and MPAS_VM.

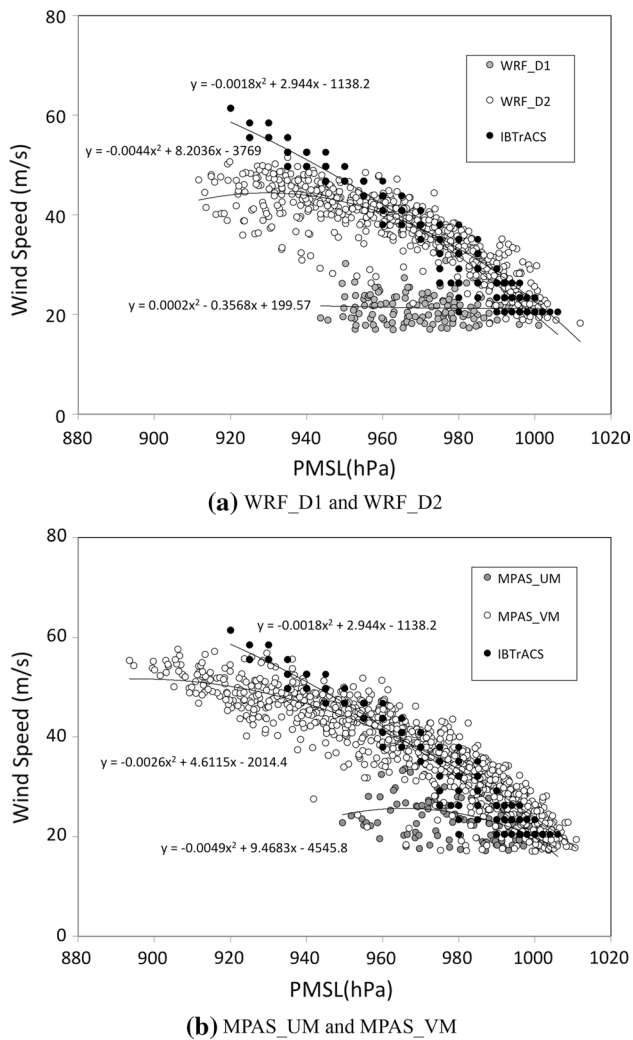


Fig. 11 Wind-pressure relationship for all 6-hourly TC points over the Northwest Pacific for **a** WRF_D1, WRF_D2, and IBTrACS, and **b** MPAS_UM, MPAS_VM, and IBTrACS. Second-order polynomial lines of best fit are shown. IBTrACS winds are converted from 10 to 1 min average using $Wind_{1min} = Wind_{10min}/0.88$

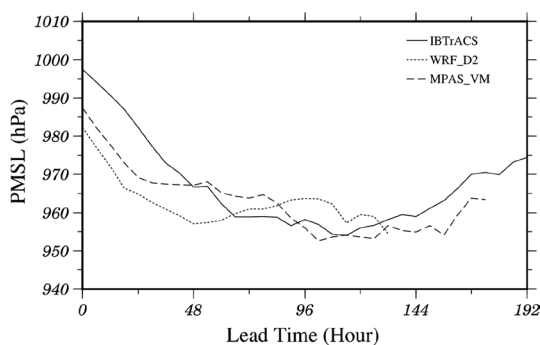


Fig. 12 Time-series of mean TC minimum PMSL (hPa) over all TCs after genesis time for the Northwest Pacific. Data are plotted when the averaging sample size is ≥ 10 TC data points and for IBTrACS, when wind speed is $\geq 17 \text{ ms}^{-1}$ for consistency with the definition of simulated TCs

Table 4 Computational cost of nine days of simulation (00Z May 1 to 00Z May 10, 2005) using the National Center for Atmospheric Research's 1.5-petaflops high-performance IBM iDataPlex cluster Yellowstone

Simulation	Total MPI tasks	Total CPU time	Elapsed time per day (s)
WRF_D1	128	128,695	112
WRF_D2	512	1,751,603	380
MPAS_UM	128	153,977	134
MPAS_VM	512	1,312,390	285

Elapsed time per day is Total CPU time/(Total MPI tasks \times 9 days)

5 Conclusion

The capacity of two different grid refinement methods (WRF nesting and MPAS variable-mesh) to capture TC activity over the Northwest Pacific is compared among a suite of simulations of the period May 2005 to April 2006. The simulations were set up to be comparable in terms of physical parameterizations, and the region and level of refinement from approximately 100 to 20 km grid spacing over the Northwest Pacific. Rather than assessing the skill of the models, this study demonstrates the capacity of a variable resolution mesh for seasonal TC simulation, and identifies potential benefits above the nesting approach to mesh refinement.

The ability to capture smooth transitions between the two resolutions varied between models. WRF nesting showed adverse influence of the nest boundary, with the boundary evident in seasonal average cloud patterns, contortions of the seasonal average mid-level jet structure, and abrupt changes in seasonal average precipitation. MPAS variable-mesh, on the other hand, showed far smoother cloud patterns, smoother mid-level jet structures comparable to reanalysis data, and no imprint of grid refinement in the seasonal average precipitation. Additionally, WRF simulations generated an anomalously strong southern hemisphere mid-latitude jet at 500 hPa over the Southwest Pacific Ocean that is likely attributable to the fixed southern domain boundary.

Precipitation totals were overestimated in both models and this wet bias appeared to be greatest over tropical regions where convective activity is dominant rather than confined to the region of high resolution in the grid refined simulations. For both models, grid refinement led to increased TC frequency in the region of refinement compared to simulations without grid refinement. Both grid refined simulations reproduced reasonable TC genesis regions, wind-pressure relationships, and mean intensification rates. However, WRF nesting appeared to adversely affect TC tracks through a contorted jet structure and steering flow associated with the nesting. MPAS variable-mesh substantially increased

TC activity over the Southern Indian and Southwest Pacific basins, outside the mesh refined region. WRF nesting, on the other hand, did not appear to substantially influence basins outside the region of grid refinement. Though not explored here, it is possible that some of the differences in seasonal climate and TC activity between WRF and MPAS may be attributed to differences in the dynamical cores (Reed and Jablonowski 2012). The role of physics, dynamics, and their interaction on variable grids and the potential simulation benefits remains to be fully explored.

Limited area models such as the WRF model have been used widely to study regional climate and high impact weather (e.g. Tulich et al. 2011; Bruyère et al. 2014; Done et al. 2013). MPAS simulations compared favorably with WRF model simulations in the capacity to capture large-scale climate features and TC activity. This study demonstrates capacity of variable mesh refinement for seasonal TC simulation and provides a foundation upon which subsequent studies may assess the skill of MPAS for capturing regional climate. Potential benefits of MPAS for regional climate simulation have been identified by reducing some of the problems associated with traditional nesting approaches to regional refinement. These benefits also come at a reduced computational cost. Table 4 summarizes the relative costs increases of the two mesh refinement techniques for the model setups used here and run on the National Center for Atmospheric Research's Yellowstone system. Ratios of total CPU time show that variable resolution MPAS increased the cost by 8.5 times that of a uniform MPAS coarse mesh, whereas the addition of the nested domain in WRF increased the cost by 13.6 times that of the parent WRF domain. There are many factors driving these differences (not quantified here) including different scaling between WRF and MPAS and the need for a global reduction in the MPAS timestep with variable mesh refinement.

Acknowledgments The National Center for Atmospheric Research is sponsored by the National Science Foundation and this work was partially supported by the Willis Research Network, the Research Partnership to Secure Energy for America, the Climatology and Simulation of Eddies/Eddies Joint Industry Project, and National Science Foundation Grant 1048829.

Open Access This article is distributed under the terms of the Creative Commons Attribution 4.0 International License (<http://creativecommons.org/licenses/by/4.0/>), which permits unrestricted use, distribution, and reproduction in any medium, provided you give appropriate credit to the original author(s) and the source, provide a link to the Creative Commons license, and indicate if changes were made.

References

- Adler RFA, Huffman GJ, Chang A, Ferraro R, Xie P-P, Janowiak J, Rudolf B, Schneider U, Curtis S, Bolvin D, Gruber A, Susskind J, Arkin P, Nelkin E (2003) The version-2 global precipitation climatology project (GPCP) monthly precipitation analysis (1979–present). *J Hydrometeorol* 4:1147–1167
- Archambault HM, Bosart LF, Keyser D, Cordeira JM (2013) A climatological analysis of the extratropical flow response to recurring western North Pacific tropical cyclones. *Mon Weather Rev* 141:2325–2346
- Bruyère CL, Done JM, Holland GJ, Fredrick S (2014) Bias corrections of global models for regional climate simulations of high-impact weather. *Clim Dyn* 43(7–8):1847–1856. doi:10.1007/s00382-013-2011-6
- Bullock OR Jr, Alapaty K, Herwehe JA, Kain JS (2015) A dynamically computed convective time scale for the Kain-Fritsch convective parameterization scheme. *Mon Weather Rev* 143:2105–2120
- Chen F, Dudhia J (2001) Coupling an advanced land surface-hydrology model with the Penn State–NCAR MM5 modeling system. Part I: model implementation and sensitivity. *Mon Weather Rev* 129:569–585
- Chen W, Jiang Z, Li L, You P (2011) Simulation of regional climate change under the IPCC A2 scenario in southeast China. *Clim Dyn* 36:491–507
- Collins WD, Rasch PJ, Boville BA, Hack JJ, McCaa JR, Williamson DL, Kiehl JT, Briegleb B (2004) Description of the NCAR Community Atmosphere Model (CAM 3.0). NCAR TECHNICAL NOTE, NCAR/TN-464+STR
- Done JM, Holland GJ, Bruyère CL, Leung LR, Suzuki-Parker A (2013) Modeling high-impact weather and climate: lessons from a tropical cyclone perspective. *Clim Change*. doi:10.1007/s10584-013-0954-6
- Done JM, Bruyère CL, Ge M, Jaye A (2014) Internal variability of North Atlantic tropical cyclones. *J Geophys Res Atmos* 119:6506–6519
- Dudhia J, Hong S-Y, Lim K-S (2008) A new method for representing mixed-phase particle fall speeds in bulk microphysics parameterizations. *J Meteorol Soc Jpn* 86:33–44
- Fowler LD, Bruyère CL, Ge M, Skamarock WC (2015) Regional climate modeling using a variable-resolution mesh in MPAS. *J Adv Model Earth Syst* (Submitted)
- Giorgi F, Bates GT (1989) The climatological skill of a regional model over complex terrain. *Mon Weather Rev* 117:2325–2347
- Harris LM, Lin S-J (2014) Global-to-regional nested grid climate simulations in the GFDL high resolution atmospheric model. *J Clim* 27:4890–4910
- Hart RE (2003) A cyclone phase space derived from thermal wind and thermal asymmetry. *Mon Weather Rev* 131:585–616
- Hirakuchi H, Giorgi F (1995) Multiyear present-day and 2× CO₂ simulations of monsoon climate over eastern Asia and Japan with a regional climate model nested in a general circulation model. *J Geophys Res* 100:D10
- Hong S-Y, Noh Y, Dudhia J (2006) A new vertical diffusion package with an explicit treatment of entrainment processes. *Mon Weather Rev* 134:2318–2341
- Huffman GJ, Bolvin DT, Nelkin EJ, Wolff DB, Adler RF, Gu G, Hong Y, Bowman KP, Stocker EF (2007) The TRMM multisatellite precipitation analysis (TMPA): quasi-global, multiyear, combined-sensor precipitation estimates at fine scales. *J Hydrometeorol* 8:38–55
- Hurrell JW, Hack J, Shea D, Caron JM, Rosinski J (2008) A new sea surface temperature and sea ice boundary dataset for the Community Atmosphere Model. *J Clim* 21:5145–5153
- Jourdain NC, Marchesiello P, Menkes CE, Lefevre J, Vincent EM, Lengaigne M, Chauvin F (2011) Mesoscale simulation of tropical cyclones in the South Pacific: climatology and interannual variability. *J Clim* 24:3–25

- Kain JS (2004) The Kain-Fritsch convective parameterization: an update. *J Appl Meteorol* 43:170–181
- Kalnay E, Kanamitsu M, Kistler R, Collins W, Deaven D, Gandin L, Iredell M, Saha S, White G, Woollen J, Zhu Y, Leetmaa A, Reynolds R, Chelliah M, Ebisuzaki W, Higgins W, Janowiak J, Mo KC, Ropelewski C, Wang J, Jenne R, Joseph D (1996) The NCEP/NCAR 40-year reanalysis project. *Bull Am Meteorol Soc* 77:437–471
- Kendon EJ, Roberts NM, Fowler HJ, Roberts MJ, Chan SC (2014) Heavier summer downpours with climate change revealed by weather forecast resolution model. *Nat Clim Change*. doi:10.1038/nclimate2258
- Klemp JB, Skamarock WC, Dudhia J (2007) Conservative split-explicit time integration methods for the compressible nonhydrostatic equations. *Mon Weather Rev* 135:2897–2913
- Knapp KR, Kruk MC, Levinson DH, Diamond HJ, Neumann CJ (2010) The international best track archive for climate stewardship (IBTrACS). *Bull Am Meteorol Soc* 91:363–376
- Knutson TR, Sirutis JJ, Vecchi GA, Garner S, Zhao M, Kim H-S, Bender M, Tuleya RE, Held IM, Villarini G (2013) Dynamical downscaling projections of twenty-first-century atlantic hurricane activity: CMIP3 and CMIP5 model-based scenarios. *J Clim* 26:6591–6617
- Kusunoki S, Yoshihara J, Yoshimura H, Noda A, Oouchi K, Mizuta R (2006) Change of Baiu rain band in global warming projection by an atmospheric general circulation model with a 20-km grid size. *J Meteorol Soc Jpn* 84:581–611
- McTaggart-Cowan R, Galarneau TJ, Bosart LF, Moore RW, Martius O (2013) A global climatology of baroclinically influenced tropical cyclogenesis. *Mon Weather Rev* 141:1963–1989
- Michalakes J, Dudhia J, Gill D, Henderson T, Klemp J, Skamarock W, Wang W (2004) The weather research and forecast model: software architecture and performance, 11th Workshop on the Use of High Performance Computing in Meteorology, United Kingdom
- Mizuta R, Yoshimura H, Murakami H, Matsueda M, Endo H, Ose T, Kamiguchi K, Hosaka M, Sugi M, Yukimoto S, Kusunoki S, Kitoh A (2012) Climate simulations using MRI-AGCM3.2 with 20-km grid. *J Meteorol Soc Jpn* 90A:233–258
- Qian JH, Seth A, Zebiak S (2003) Reinitialized versus continuous simulations for regional climate downscaling. *Mon Weather Rev* 131:2857–2874
- Ray P, Zhang C, Moncrieff MW, Dudhia J, Caron JM, Leung LR, Bruyere C (2011) Role of the atmospheric mean state on the initiation of the Madden-Julian oscillation in a tropical channel model. *Clim Dyn* 36:161–184
- Reed KA, Jablonowski C (2012) Idealized tropical cyclone simulations of intermediate complexity: a test case for AGCMs. *J Adv Model Earth Syst* 4:M04001. doi:10.1029/2011MS000099
- Ringler T, Thuburn J, Klemp J, Skamarock W (2010) A unified approach to energy conservation and potential vorticity dynamics on arbitrarily structured C-grids. *J Comput Phys* 229:3065–3090
- Sasaki H, Murata A, Hanafusa M, Oh'izumi M, Kurihara K (2011) Reproducibility of present climate in a non-hydrostatic regional climate model nested within an atmosphere general circulation model. *SOLA* 7:173–176
- Skamarock WC, Klemp JB, Dudhia J, Gill DO, Barker DM, Wang W, Powers JG (2008) A description of the advanced research WRF Version 3, NCAR TECHNICAL NOTE, NCAR/TN-475+STR
- Skamarock WC, Klemp JB, Duda MG, Fowler LD, Park S-H, Ringler TD (2012) A multi-scale nonhydrostatic atmospheric model using centroidal voronoi tessellations and C-grid staggering. *Mon Weather Rev* 140:3090–3105
- Suzuki-Parker A (2012) An assessment of uncertainties and limitations in simulating tropical cyclones, Springer Thesis XIII:78
- Thuburn J, Ringler T, Klemp J, Skamarock W (2009) Numerical representation of geostrophic modes on arbitrarily structured C-grids. *J Comput Phys* 228:8321–8335
- Tulich SN, Kiladis GN, Suzuki-Parker A (2011) Convectively coupled Kelvin and easterly waves in a regional climate simulation of the tropics. *Clim Dyn* 36:185–203
- Wang Y, Leung LR, McGregor JL, Lee D-K, Wang W-C, Ding Y, Kimura F (2004) Regional climate modeling: progress, challenges, and prospects. *J Meteorol Soc Jpn* 82:1599–1628
- Wehner MF, Reed K, Li F, Prabhat, Bacmeister J, Chen C-T, Paciorek C, Gleckler P, Sperber K, Collins WD, Gettelman A, Jablonowski C, Algieri C (2014) The effect of horizontal resolution on simulation quality in the Community Atmospheric Model, CAM5.1. *J Adv Model Earth Syst*. doi:10.1002/2013MS000276
- Williamson DL, Kiehl JT, Ramanathan V, Dickinson RE, Hack JJ (1987) Description of the NCAR Community Climate Model (CCM1). NCAR Technical Note NCAR/TN-285+STR
- Zarzycki CM, Jablonowski C (2014) A multidecadal simulation of Atlantic tropical cyclones using a variable-resolution global atmospheric general circulation model. *J Adv Model Earth Syst* 6:805–828
- Zarzycki CM, Jablonowski C, Thatcher DR, Taylor MA (2015) Effects of localized grid refinement on the general circulation and climatology in the Community Atmosphere Model. *J Clim* 28:2777–2803